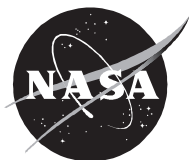NASA/CR-2002-211654
ICASE Report No. 2002-14

Simulation of Embedded Streamwise Vortices on a Flat Plate

Brian G. Allan
ICASE, Hampton, Virginia

Chung-Sheng Yao and John C. Lin
NASA Langley Research Center, Hampton, Virginia

May 2002

Report Documentation Page

Report Date	Report Type	Dates Covered (from... to)
00MAY2002	N/A	-

Title and Subtitle	Contract Number
Simulation of Embedded Streamwise Vortices on a Flat Plate	
	Grant Number
	Program Element Number

Author(s)	Project Number
Boris Diskin,James L. Thomas	
	Task Number
	Work Unit Number

Performing Organization Name(s) and Address(es)	Performing Organization Report Number
ICASE Mail Stop 132C NASA Langley Research Center Hampton, VA 23681-2199	

Sponsoring/Monitoring Agency Name(s) and Address(es)	Sponsor/Monitor's Acronym(s)
	Sponsor/Monitor's Report Number(s)

Distribution/Availability Statement
Approved for public release, distribution unlimited

Supplementary Notes
ICASE Report No. 2002-14

Abstract
see report

Subject Terms

Report Classification	Classification of this page
unclassified	unclassified

Classification of Abstract	Limitation of Abstract
unclassified	SAR

Number of Pages
19

The NASA STI Program Office . . . in Profile

Since its founding, NASA has been dedicated to the advancement of aeronautics and space science. The NASA Scientific and Technical Information (STI) Program Office plays a key part in helping NASA maintain this important role.

The NASA STI Program Office is operated by Langley Research Center, the lead center for NASA's scientific and technical information. The NASA STI Program Office provides access to the NASA STI Database, the largest collection of aeronautical and space science STI in the world. The Program Office is also NASA's institutional mechanism for disseminating the results of its research and development activities. These results are published by NASA in the NASA STI Report Series, which includes the following report types:

- TECHNICAL PUBLICATION. Reports of completed research or a major significant phase of research that present the results of NASA programs and include extensive data or theoretical analysis. Includes compilations of significant scientific and technical data and information deemed to be of continuing reference value. NASA's counterpart of peer-reviewed formal professional papers, but having less stringent limitations on manuscript length and extent of graphic presentations.

- TECHNICAL MEMORANDUM. Scientific and technical findings that are preliminary or of specialized interest, e.g., quick release reports, working papers, and bibliographies that contain minimal annotation. Does not contain extensive analysis.

- CONTRACTOR REPORT. Scientific and technical findings by NASA-sponsored contractors and grantees.

- CONFERENCE PUBLICATIONS. Collected papers from scientific and technical conferences, symposia, seminars, or other meetings sponsored or cosponsored by NASA.

- SPECIAL PUBLICATION. Scientific, technical, or historical information from NASA programs, projects, and missions, often concerned with subjects having substantial public interest.

- TECHNICAL TRANSLATION. English-language translations of foreign scientific and technical material pertinent to NASA's mission.

Specialized services that complement the STI Program Office's diverse offerings include creating custom thesauri, building customized data bases, organizing and publishing research results . . . even providing videos.

For more information about the NASA STI Program Office, see the following:

- Access the NASA STI Program Home Page at *http://www.sti.nasa.gov*

- Email your question via the Internet to help@sti.nasa.gov

- Fax your question to the NASA STI Help Desk at (301) 621-0134

- Telephone the NASA STI Help Desk at (301) 621-0390

- Write to:
  NASA STI Help Desk
  NASA Center for AeroSpace Information
  7121 Standard Drive
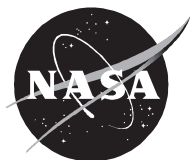 Hanover, MD 21076-1320

Simulation of Embedded Streamwise Vortices on a Flat Plate

Brian G. Allan
ICASE, Hampton, Virginia

Chung-Sheng Yao and John C. Lin
NASA Langley Research Center, Hampton, Virginia

ICASE
NASA Langley Research Center
Hampton, Virginia

Operated by Universities Space Research Association

May 2002

SIMULATION OF EMBEDDED STREAMWISE VORTICES ON A FLAT PLATE

BRIAN G. ALLAN[*], CHUNG-SHENG YAO[†], AND JOHN C. LIN[‡]

Abstract. Numerical simulations of a single low-profile vortex generator vane, which is only a small fraction of the boundary-layer thickness, have been performed for flows over a flat plate. The numerical simulations were computed by solving the steady-state solution to the Reynolds-averaged Navier-Stokes equations. The vortex generating vane results were evaluated by comparing the strength and the trajectory of the streamwise vortex to experimental particle image velocimetry measurements. From the numerical simulations it was observed that the Shear-Stress Transport (SST) turbulence model resulted in a better prediction of the streamwise peak vorticity and trajectory when compared to the Spalart-Allmaras (SA) turbulence model. It is shown in this investigation that the estimation of the turbulent eddy viscosity near the vortex core was very high using the SA model as compared to the SST model. Even though the numerical simulations were able to predict the trajectory of the streamwise vortex, the initial magnitude and decay of the peak streamwise vorticity were significantly under predicted. A comparison of the positive circulation associated with the streamwise vortex showed that while the numerical simulations produced a more diffused vortex, the vortex strength compared very well to the experimental observations. A grid resolution study was also performed showing that the diffusion of the vortex was not a result of insufficient grid resolution. Comparisons were also made between a fully modeled trapezoidal vane with finite thickness to a simply modeled rectangular thin vane. These comparisons showed that the simply modeled rectangular vane produced a streamwise vortex which had a strength and trajectory very similar to the fully modeled trapezoidal vane.

Key words. Reynolds-averaged Navier-Stokes, vortex generator, flow control

AMS subject classification. Applied Numerical Mathematics, Controls

1. Introduction. Incorporation of low-profile vortex generating (VG) devices, in the design of compact aircraft inlets, has demonstrated significant improvements in turbofan engine-face flow distortion [4]. Recently Hamstra et al. [4] have shown a comparison between a computational fluid dynamics (CFD) analysis of a compact inlet flow, with VG vanes, to experimental results. They showed that the CFD simulations are able to accurately predict the inlet surface pressure and the engine-face flow distortion measured in experiments. These CFD simulations used a simplified VG vane model, described by Bender et al. [1], eliminating the need to model the vane geometry, resulting in a reduced computational cost.

The model described by Bender et al. [1] models a VG vane by introducing a source term in the momentum and energy equations. The strength of the source term is adjusted based on the local flow and represents the side force generated by a vane or row of vanes. The success of this model for internal inlet flows shows that it may be possible to simulate the effects of VG vanes for other types of flows using a boundary condition approach rather than fully gridding the flow control devices. The validation of the Bender et al. [1] model was made using an integral of the cross flow kinetic energy far down stream of the vanes at the inlet exit. In an effort to achieve a more detail evaluation of this and other types of reduced CFD models, numerical simulations of a single, fully grided, low-profile VG vane on a flat plate were performed.
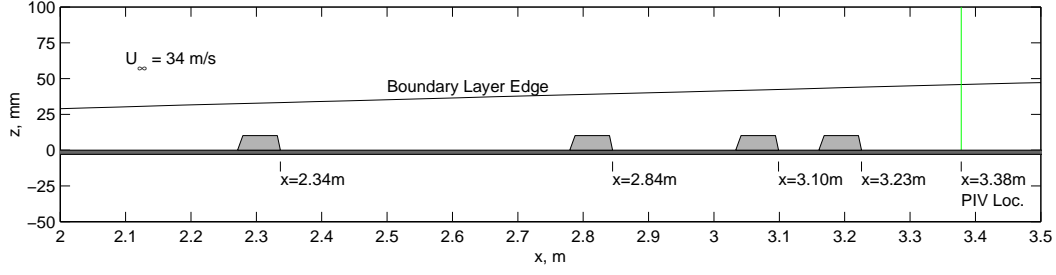

FIG. 2.1. *VG vanes and PIV measurement locations on the flat plate where x is measured from the leading edge of the plate. This figure also shows the profile of the baseline boundary layer edge with respect to the vane height.*

The numerical simulations of a single vane on a flat plate were generated in collaboration with wind tunnel experiments performed at NASA Langley. This experimental data will be used to assess the flow predicted by a Reynolds-averaged Navier-Stokes (RANS) flow solver for a single VG vane case. Evaluation of numerical and experimental data will provide detailed insight into the physics of the flow around and downstream of the VG vane. The insight gained from this investigation can then be used to justify future modeling choices for the development of a reduced CFD model for VG vanes.

2. Wind Tunnel Experiments. Wind tunnel experiments of a single vane submerged within a turbulent boundary layer over a flat plate were conducted in NASA Langley's 20×28-Inch Shear Flow Tunnel. Detailed flow field velocity measurements were taken in crossflow planes downstream of the VG device using a three-dimensional stereo digital Particle Image Velocimetry (PIV) system, where all three components of velocity were obtained through stereoscopic vector reconstruction, as describe by Yao et al. [12]. The assembly of this PIV flow field data, for various distances downstream of the VG vane, is then used to characterize the evolution of the streamwise vortex embedded in a boundary layer.

The experiments were conducted at a freestream velocity, U_∞, of $34\,m/s$. A splitter plate was mounted above the test section floor and its leading edge was tripped to force a fully developed turbulent boundary layer downstream. The PIV data was taken at a fixed crossflow plane station located $3.38\,m$ downstream from the leading edge of the plate. Four flow field surveys were taken where each survey consisted of placing an individual VG at a different position upstream of the PIV measuring location. Figure 2.1 shows the location of the PIV measuring station ($x = 3.38\,m$) as well as the four VG locations at $x = 3.23\,m$, $3.10\,m$, $2.84\,m$, and $2.34\,m$ that correspond to a distance of $15.2\,cm$, $27.9\,cm$, $53.3\,cm$, and $104\,cm$ from the vane trailing edge to the measurement location, respectively. This figure also shows the relative height of the boundary layer for the baseline flat plate flow with the VG vane removed.

The baseline boundary-layer thickness, δ, at the vane locations varies from $33\,mm$, at the most upstream location ($x = 2.34\,m$), to $45\,mm$, the farthest downstream vane location ($x = 3.23\,m$). The VG vane used for this experiment has a height, h, of $10.2\,mm$, which results in a variation of h/δ between 0.31 and 0.23. The vane has a length, L, of $71\,mm$ resulting in a L/h of 7. The vane has a trapezoidal planform geometry similar in shape to that of the trapezoidal wing-micro VGs reported by Lin [7].

Using this type of experimental setup the boundary layer thickness and velocity profile vary at the four different VG locations. The objective of this study is to characterize the trajectory of the streamwise vortex and the flow field downstream of the VG vane. Thus, this variation in the boundary layer profile is unwanted. It will be shown later that this variation has a small effect on the data point for the most upstream vane location and a very slight effect on the data points for the other three VG locations.
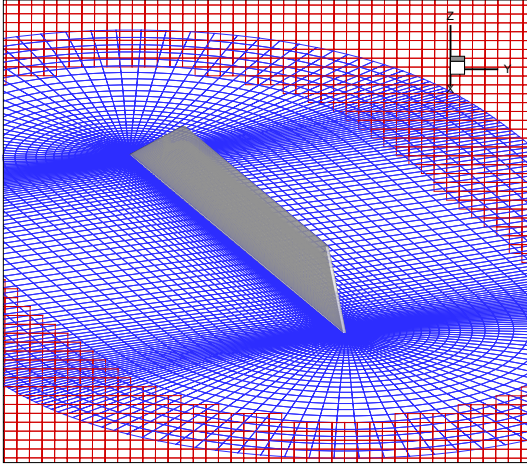
2

FIG. 3.1. *Overset grids for the thick trapezoidal low-profile vortex generator vane.*
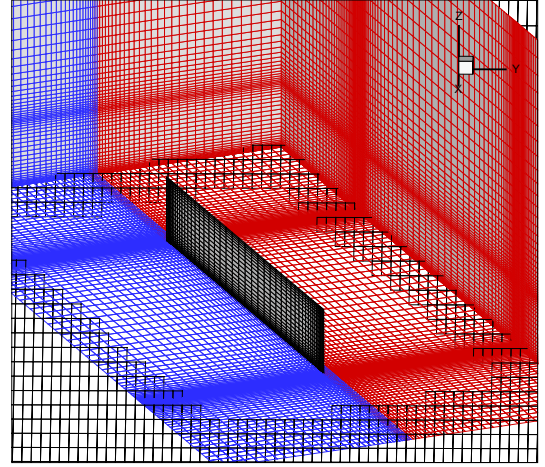

FIG. 3.2. *Overset grids for thin rectangular thin low-profile vortex generator vane.*

3. Numerical Modeling. The steady-state flow field about a single vortex generator vane on a flat plate was computed using the flow solver code, OVERFLOW [2, 6], developed at NASA. This code solves the compressible RANS equations using the diagonal scheme of Pulliam and Chaussee [9]. The RANS equations are solved on structured grids using the overset grid framework of Steger et al. [11]. This overset grid framework allows for the use of structured grids for problems which have complex geometries. To improve the convergence of the steady-state solution, the OVERFLOW code also includes a low-Mach preconditioning option and a multigrid acceleration routine, which were implemented for the numerical simulations.

The OVERFLOW code has several options for turbulence models. This investigation focuses on the one-equation model of Spalart and Allmaras [10] (SA) and the two-equations (k-ω) Shear-Stress Transport (SST) model of Menter [8]. The SA turbulence model is popular because of its ease of implementation, relative low cost, and good performance. The SST model is a k-ω two-equation model which accounts for the transport of the principal shear stress in adverse pressure gradients boundary layers. Both models are well known and are currently used to solve problems relating to aerospace vehicle applications.

The numerical simulations were performed using the parallel version of the OVERFLOW code developed by Jespersen [5]. This code uses the Message-Passing Interface (MPI) and can run on a tightly-coupled parallel machine or a network of workstations. The code distributes zones to individual processors and can split larger individual zones across multiple processors by using a pipelined Gaussian elimination method. Splitting the larger zones across multiple processors significantly improves the load-balancing for problems with zones of varying size.

The structured overset grids were generated using the Chimera Grid Tools package [3]. Figure 3.1 shows a close-up view of the overset grids near the trapezoidal vane on the flat plate. This vane was modeled with a finite thickness and round edges using an O-grid around the vane and a cap grid for the top edge. The O-grid is overset on a fine Cartesian block grid which captures the vortex wake. This fine block grid is then overset on to a coarser Cartesian block grid which models the flat plate. In Fig. 3.1 a blanked out region on the flat plate grid can be seen where the the flow field is resolved by the finer vane grids. The volume grids around the vane were generated using the hyperbolic grid generator found in the Chimera Grid Tools package.

Figure 3.2 shows a set of two grids which overlap and model a thin vane which has an area equal to the trapezoidal vane. This grid system does not account for the thickness of the vane but is much simpler to generate and can easily be modified to increase or decrease grid resolution. Comparisons between the thin vane model will be made to the more
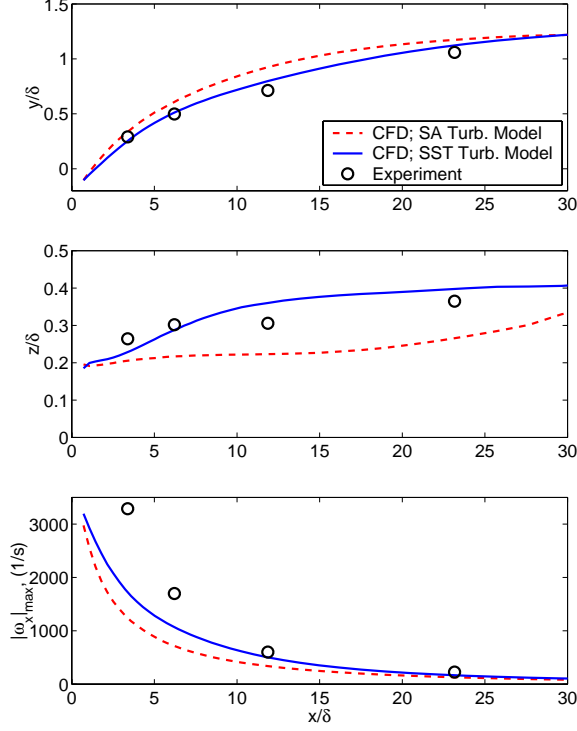
FIG. 4.1. *Trajectory and magnitude comparisons of the peak streamwise vorticity, using the SA and SST turbulence models, to the experimental data for the vane at* $\alpha = 23^o$ *where* $\delta = 45\,mm$.
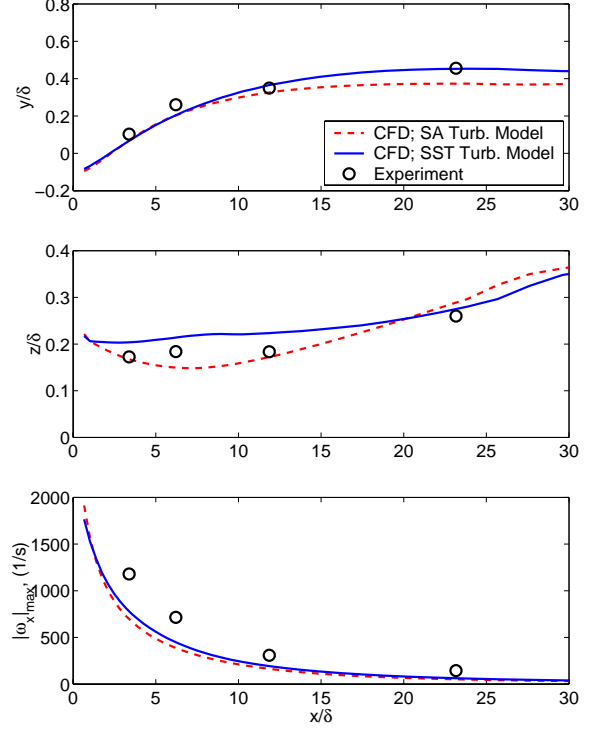
FIG. 4.2. *Trajectory and magnitude comparisons of the peak streamwise vorticity, using the SA and SST turbulence models, to the experimental data for the vane at* $\alpha = 10^o$ *where* $\delta = 45\,mm$.

complex trapezoidal vane.

4. Results and Discussions. Numerical simulations of a low-profile vortex generating vane on a flat plate are performed and compared to the experimental results. For both the experiments and simulations, the vane is positioned at device angels, α, of $10°$ and $23°$ with respect to the freestream flow. The vortex generating vane is then characterized by the trajectory of the streamwise vortex core, decay of the peak vorticity, and positive circulation.

4.1. Experimental Results. The PIV system collected flow filed data on a grid which has 40 points in the spanwise direction and 33 points in the vertical direction. The data points are evenly spaced at approximately $1.7\,mm$ in the vertical direction and $2.2\,mm$ in the spanwise direction. The three components of mean velocity are collected at each grid point by the PIV system. Using the velocity data, the streamwise component of the vorticity can be computed. The streamwise vorticity data was then used to plot the trajectory and decay of the peak vorticity as well as the positive circulation. Subsequently, this information was used to evaluate the numerical results given below.

4.2. Numerical Results. The finite thickness trapezoidal vane (shown in Fig. 3.1) models the shape and thickness of the actual vane used in the wind tunnel experiments. This model of the vane was used to simulate the flow of the vane on a flat plate at device angles of $10°$ and $23°$ with respect to the freestream flow of $34\,m/s$. Numerical simulations are made using both SA and SST turbulence models. Unlike the experiments, the numerical simulations will evaluate the trajectory of the streamwise vortex by positioning the vane at a fixed ($x = 3.23\,m$) location. The flow from this vane location is then compared to the experimental data where the measurement location is fixed and the vane is moved. The error introduced by this approach will be quantified by comparing the numerical simulations for each vane location.

Figure 4.1 shows a comparison of the peak streamwise vorticity for the $23°$ vane case between the experimental
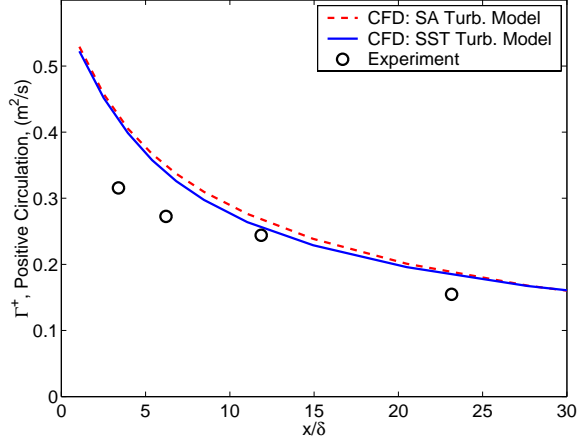
FIG. 4.3. *Comparison of positive circulation for* α = 23° *where* δ = 45 *mm.*

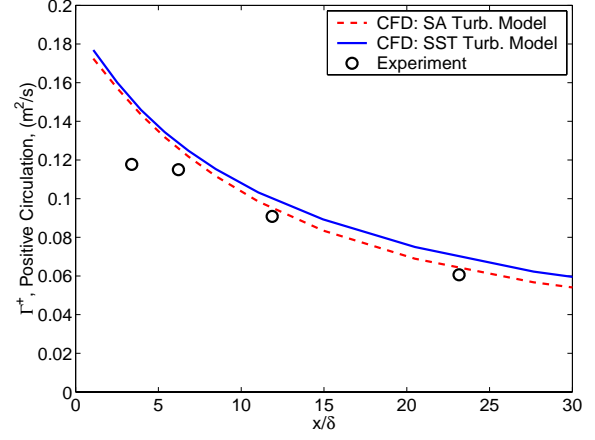

FIG. 4.4. *Comparison of positive circulation for* α = 10° *where* δ = 45 *mm.*

data and the numerical simulations using the SA and SST turbulence models. Comparing the magnitude of the peak vorticity, it can be seen that both simulations under predict the initial magnitude and decay rates. The SST and SA simulations both predict nearly the same initial peak vorticity. However, the SA simulation shows a much faster decay of the peak vorticity as compared to the SST simulation.

The path of the vortex core for the 23° vane case is also shown in Fig. 4.1. The spanwise, *y*, trajectory of the vortex core shows that the SST simulation compares very well with experiment and that the SA model tends to over predict the path in the cross flow direction. The location of the center of the vortex in the vertical direction, *z*, shows that the SST model captures the vertical trajectory where the SA model shows a slight under prediction of the vortex height. The SST model compares well with the experiments up to $x/\delta = 5$ and does not capture the flat spot in the vortex trajectory at $x/\delta = 10$ as seen in the experimental data.

Using the SA and SST turbulence models, the flow was simulated for a single vane at a device angle of 10°. The magnitude and trajectory of the peak core vorticity is shown in Fig. 4.2 with a comparison to the experimental data. This comparison shows similar trends seen in the 23° case. The vertical location of the vortex center does compare well to the experimental data for both the SST and SA models. The spanwise path of the vortex compares very well with the experiment when using the SST model and is slightly under predicted for the SA simulation. The magnitude of the peak vorticity is still under predicted by the numerical simulations when compared to the experimental data. Unlike the 23° vane case, the peak vorticity predicted by the SA simulation is only slightly lower than the peak vorticity for the SST simulation.

The positive circulation, Γ^+, about the streamwise vortex was computed for the 23° and 10° vane cases and shown in Figs. 4.3 and 4.4, respectively. The circulation was computed by integrating the positive streamwise vorticity around the vortex. In an effort to make a fair comparison between the numerical and experimental data, the velocity field was interpolated onto a grid similar in resolution to the experimental PIV data. The positive circulation about the streamwise vortex was then computed using this interpolated velocity data by calculating the streamwise vorticity and integrating the positive vorticity.

Figure 4.3 compares of the positive circulation between the numerical simulations and experimental data for 23° case. This comparison shows that the circulation computed from the experimental data is lower than the numerical simulation for the first two data points. The circulation values compare much better for the last two experimental data points. This figure also shows a comparison between the circulation for the SA and SST turbulence model
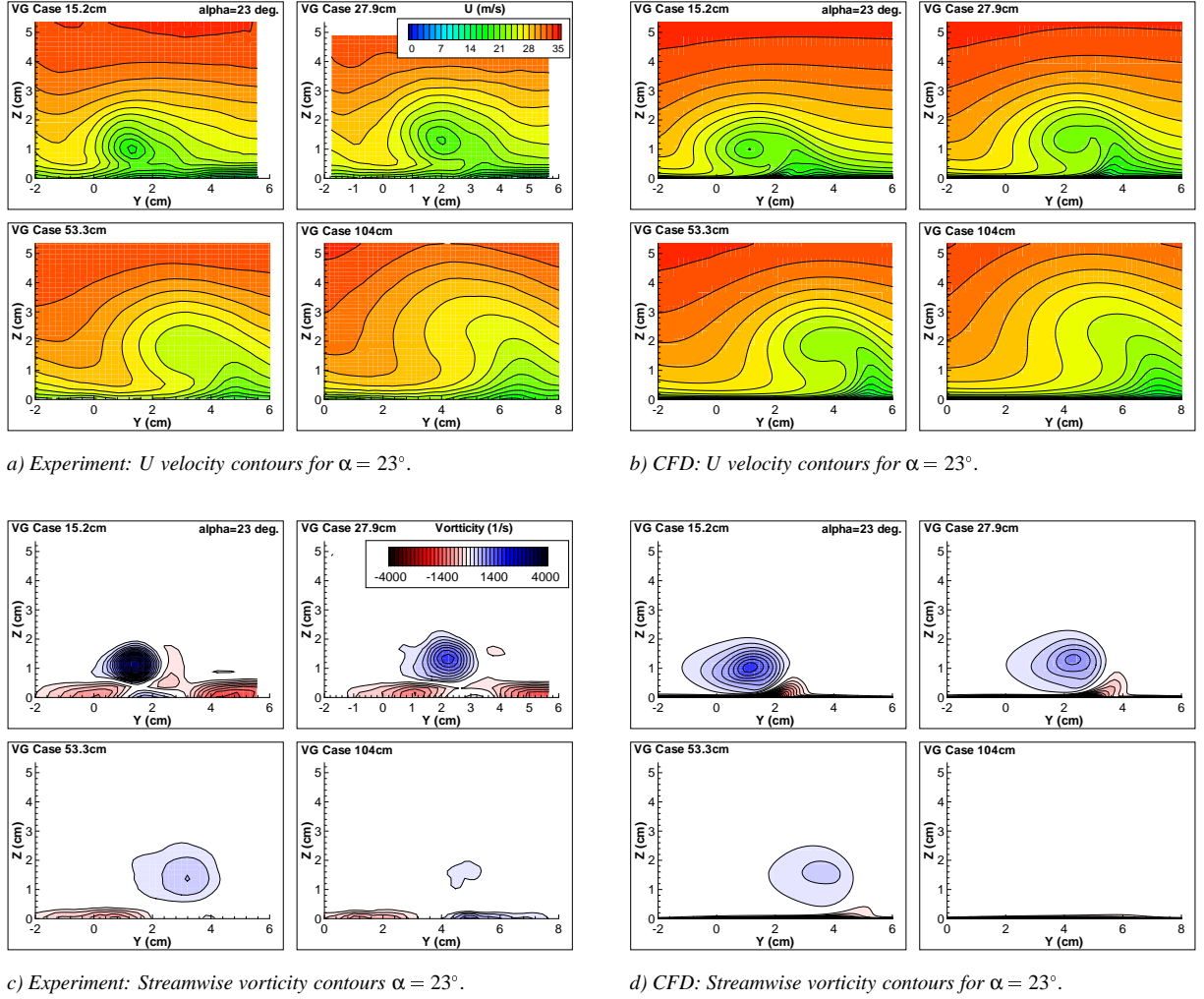
a) Experiment: U velocity contours for α = 23°.

b) CFD: U velocity contours for α = 23°.

c) Experiment: Streamwise vorticity contours α = 23°.

d) CFD: Streamwise vorticity contours for α = 23°.

FIG. 4.5. *A comparison between CFD and experiment for the* 23° *vane case at four different locations downstream of the vane.*

simulations. This comparison indicates that the circulation is about the same when using the SA and SST turbulence models. Therefore, simulations using either turbulence model generate a streamwise vortex of equal strength and with a similar rate of decay. The 10° case is given in Fig. 4.4 and shows how the circulation from the experimental data compares well to the numerical simulations except for the first data point. This figure also shows how the circulation using the SA and SST turbulence models are almost the same. As in the 23° case, the 10° case displays a vortex strength and decay rate for the two turbulence models which are nearly the same.

The comparison of circulation for the numerical simulations using the SA and SST turbulence models show how they both produce a streamwise vortex with the same strength. This indicates that the difference in the peak vorticity is not related to the initial strength of the streamwise vortex but instead to the diffusion of the vortex. Specifically the comparisons of peak vorticity show that the SA model diffuses the streamwise vortex faster than the SST model. The low peak vorticity close to the vanes indicate that the numerical simulations tend to diffuse the embedded streamwise vortex much faster than the vortex observed in the experiments.

Figures 4.5 and 4.6 show both the streamwise velocity and streamwise vorticity contours for the vortex generating vane at device angles 23° and 10°, respectively. These figures compare the numerical simulations using the SST turbulence model to the experimental PIV data. The 23° case in Fig. 4.5 shows how the streamwise velocity is reduced
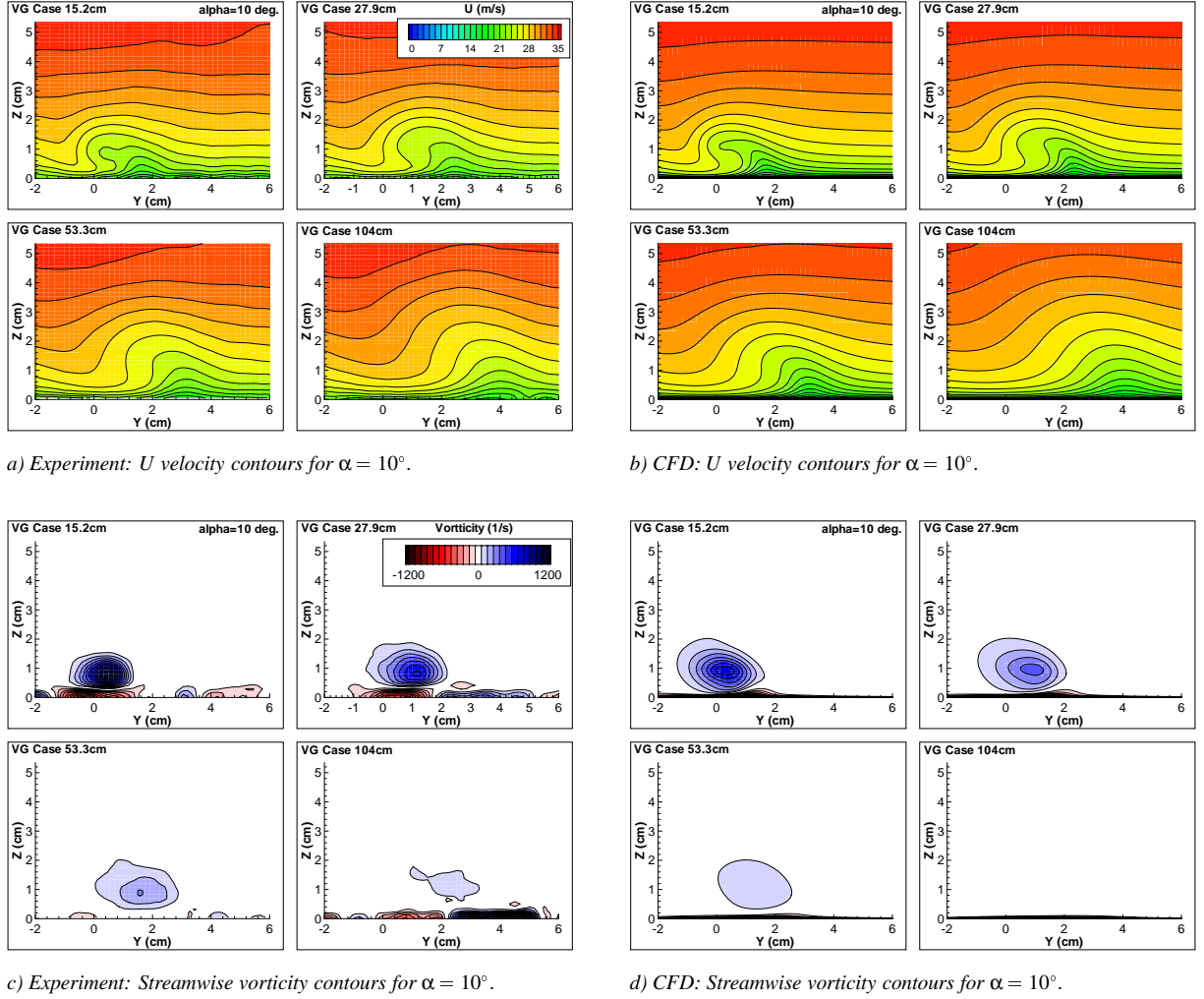
a) Experiment: U velocity contours for $\alpha = 10°$.

b) CFD: U velocity contours for $\alpha = 10°$.

c) Experiment: Streamwise vorticity contours for $\alpha = 10°$.

d) CFD: Streamwise vorticity contours for $\alpha = 10°$.

FIG. 4.6. *A comparison between CFD and experiment for the $10°$ vane case at four different locations downstream of the vane.*

at the core of the vortex. The streamwise velocity contours also show the vortex core inside the boundary layer where the top most contour line gives an estimate of the boundary layer edge. The velocity contours located $15.2\,cm$ and $27.9\,cm$ downstream from the vane show a vortex which is much more concentrated in the experiment data than in the numerical simulations. The velocity contours $53.3\,cm$ and $104\,cm$ downstream of the vane show a better comparison between the experiment and CFD. The streamwise vorticity contours also indicate a more concentrated vortex at $15.2\,cm$ and $27.9\,cm$ downstream for the experimental data as compared to the numerical results. The contour plots of vorticity also show a vortex which is more circular in the experimental results than the numerical simulations. Farther downstream, the vorticity contours at $53.3\,cm$ and $104\,cm$ from the vane compare much better where the magnitude of the peak vorticity, as was shown in Fig. 4.1, compares more favorably.

The contours for the $10°$ vane case are shown in Fig. 4.6 where the velocity and vorticity contours between the experiment and simulation compare better than the $23°$ vane case. There is a small difference in the streamwise velocity at the $15.2\,cm$ and $27.9\,cm$ downstream locations but overall the velocity contours compare well. The vorticity contours in Fig. 4.6 do show a more concentrated vortex at the $15.2\,cm$ and $27.9\,cm$ locations for the experiment as would be expected knowing the difference in the peak vorticity given in Fig. 4.2. The vorticity contours also show a rounder vortex for the experimental PIV data as compared to the oblong vortex seen in the CFD contours. Overall the
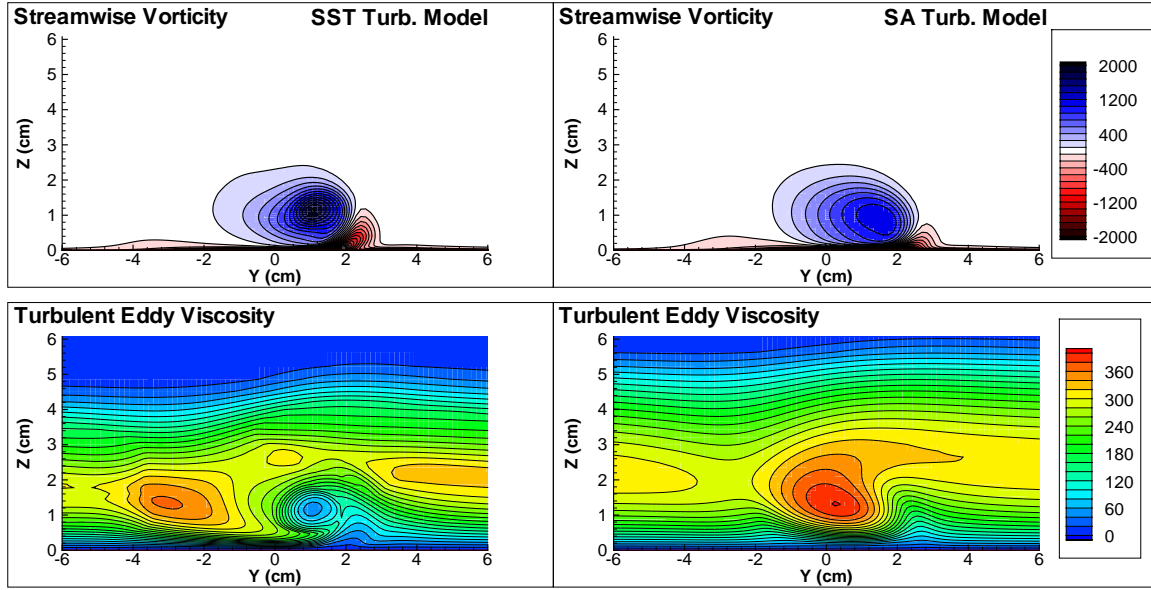
FIG. 4.7. *Contour plots of the streamwise vorticity and the turbulent eddy viscosity, μ_t, for the trapezoidal vane using the SA and SST turbulence models.*

streamwise vorticity contours for the $10°$ case compare better with the experimental results than the $23°$ case.

4.2.1. Turbulent Eddy Viscosity Effects. To better understand the difference between the numerical results using the SA and SST turbulent models, contour plots of the streamwise vorticity and turbulent eddy viscosity are shown in Fig. 4.7. These contour plots show the streamwise vortex $15.2\,cm$ downstream from the trailing edge of the VG vane at $\alpha = 23°$. From the vorticity plots it can been seen that the simulation using the SST model has a much higher peak vorticity and therefore a much more concentrated vortex. In an effort to explain the difference in the two turbulence models, a contour plot of the turbulent eddy viscosity, μ_t, generated by the turbulent models, are shown in Fig. 4.7. A comparison of these contours show that the SA model generates a peak μ_t of 400 very close to the core of the vortex. The SST model on the other hand has a minimum μ_t of 50 near the center of the vortex. This could explain why the peak vorticity using the SA model is lower than the SST model. The higher value of μ_t will tend to dissipate the concentration of the vorticity thus reducing the peak vorticity of the vortex. The μ_t generated by the SST model does show a large zone just to the left of the vortex which has a peak μ_t of 360. The distribution of the μ_t may also explain why the vortex in the numerical simulations are oblong and not circular as seen in the experimental PIV data.

4.2.2. Simplified Vane Geometry. To see how the simplification of vane geometry effects the streamwise vortex, a comparison between the fully modeled, thick trapezoidal vane, (shown in Fig. 3.1) was made to the thin rectangular vane (shown in Fig. 3.2). The dimensions of the rectangular vane were chosen such that the trapezoidal and rectangular vanes would have the same height with equal areas. Thus the height of the thin rectangular vane was $10.2\,mm$ and had a chord length of $59.4\,mm$. The thin rectangular vane simulations have the same flow conditions as the trapezoidal vane using the SST turbulence model with $\alpha = 23°$ and $10°$. Figures 4.8 and 4.9 shows a comparison between the trajectory and peak vorticity for the thick trapezoidal vane and the thin rectangular vane at $\alpha = 23°$ and $10°$, respectively. These figures shows how the thin rectangular vane model compares very well to the fully grided thick trapezoidal vane. There is a slight difference in the spanwise and vertical vortex location for the $\alpha = 23°$ case. However the decay of the peak vorticity for the two simulations are almost identical. Figures 4.10 and 4.11 show the positive circulation comparisons between the thick and thin vanes. These figures reveal how the strength of the streamwise vortex for the $\alpha = 23°$ case
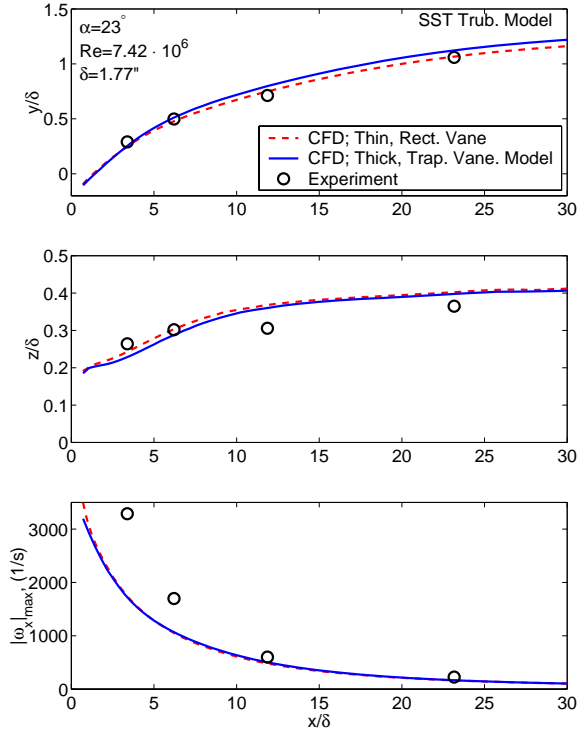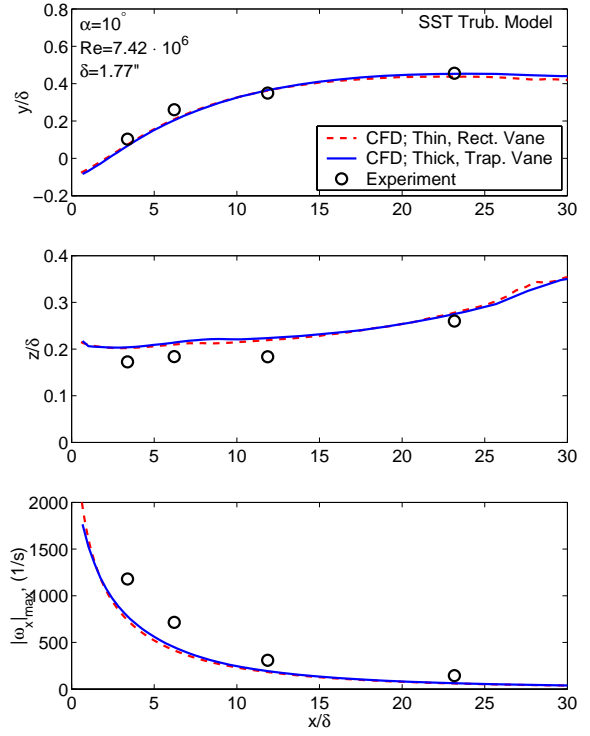
8

FIG. 4.8. *Trajectory and magnitude comparisons of the peak streamwise vorticity, using the SST turbulence model, between the fully model trapezoidal vane and the rectangular thin vane at* $\alpha = 23°$.

FIG. 4.9. *Trajectory and magnitude comparisons of the peak streamwise vorticity, using the SST turbulence model, between the fully model trapezoidal vane and the rectangular thin vane at* $\alpha = 10°$.
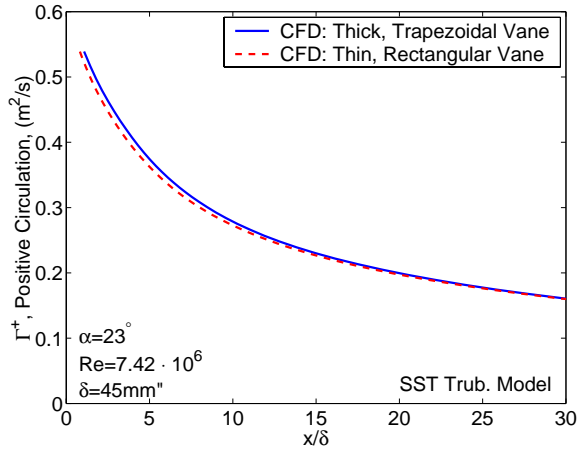

FIG. 4.10. *Circulation comparison between the fully model trapezoidal thick, vane and the rectangular, thin vane at* $\alpha = 23°$.
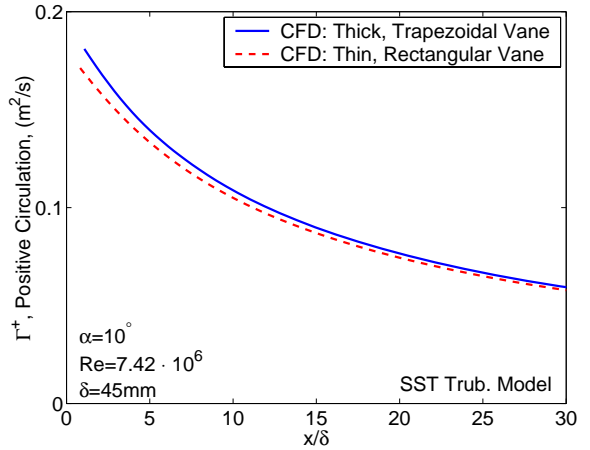

FIG. 4.11. *Circulation comparison between the fully model trapezoidal, thick vane and the rectangular, thin vane at* $\alpha = 10°$.

are almost the same where the positive circulation for the thin vane is slightly lower than the thick vane. Figure 4.11 shows that the strength of the thin vane for $\alpha = 10°$ is smaller than the thick vane for short distances downstream from the vane location but then improves for distances farther downstream. Overall the thin vane compares very well with the fully modeled thick trapezoidal vane. The thin vane grids have approximately $230,000$ grid points as oppose to the fully modeled vane which has over 1.5 million grid points. Considering the small differences in the trajectory of the
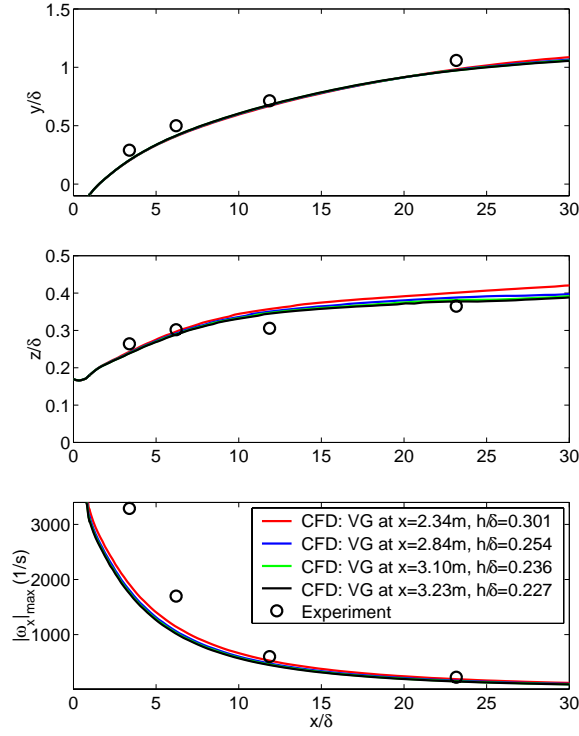
FIG. 4.12. *Trajectory and magnitude comparisons of the peak streamwise vorticity, using the SST turbulence model, for four different vane locations where* $\delta = 45\,mm$.

streamwise vortex between the thin rectangular vane and the fully grided trapezoidal vane, it would seem more cost effective to use the simplified thin vane grids rather than the fully modeled trapezoidal vane.

4.2.3. Effects of Boundary Layer Height. As a result of the fixed PIV measurement location, the vane was moved to different distances upstream in order study the evolution of the embedded vortex. Figure 2.1 shows the scaled drawing of the four different vane locations with respect to the baseline boundary layer thickness, δ, and the PIV measurement location. Since the vane geometry was held constant during the experiments, the vane height to boundary layer thickness ratio varies as the vane is moved to different locations along the flat plate. At the most upstream location, $h/\delta = 0.30$, and at the farthest downstream vane position, $h/\delta = 0.23$. In order to get an estimate of this effect on the experimental data, four numerical simulations were performed positioning the vane in the same locations as in the experiments. The trajectory and peak vorticity of the streamwise vortex from these simulations are shown in Fig. 4.12 where x/δ is the distance downstream from the trailing edged of the vane. These numerical simulations used the rectangular vane grids at $\alpha = 23°$ with the SST turbulence model.

From Fig. 4.12 it can be seen that there are small differences in the trajectories and decay rate of the peak vorticity. The spanwise trajectory for the four different vane locations show only a very slight difference. The vertical position of the vortex core does show a variation of the core height. This difference is very small for short distances downstream from the vane and becomes larger for longer distances. Since the vortex size will grow with the boundary layer thickness, this variation could be related to the boundary layer growth rate which is greatest for the most upstream vane position.

The plot of the peak streamwise vorticity does show larger values for the most upstream vane. However the differences between the experimental data and numerical simulations for the peak vorticity are much greater than the differences in vane location for distances less than $x/\delta = 10$. Also since the numerical simulations that were used to

TABLE 4.1

A comparison of the peak vorticity (1/s) between the numerical simulations and experimental PIV data. The numerical simulations are performed by positioning the vane at the same locations on the flat plate as in the experiment showing the variance in the peak vorticity at a given distance downstream of the vane. The bold numbers in the CFD data correspond to the peak vorticity for the same vane location and downstream distance as performed in the experiment.

CFD Data	Distance downstream from vane, (cm)			
Vane Loc. (m)	15.2	27.9	53.3	104
x=2.34	1911	1143	527	**190**
x=2.84	1804	1060	**476**	163
x=3.10	1764	**1030**	457	153
x=3.23	**1745**	1016	448	148
Exp. Data	3290	1700	600	224

compare with the experimental data are for a vane at $x = 2.23\,m$, the first data point $15.2\,cm$ downstream from the vane, exactly matches the experimental vane location on the flat plate. As the data points become farther downstream from the vane, the h/δ ratio between the experiments and numerical simulations becomes greater. Table 4.1 shows the peak vorticity for the numerical simulations for the four vane locations along with the peak vorticity for the experiment. The bold values in the CFD data are the values which correspond to the numerical simulations which exactly match the experimental setup at that data point. This table shows that the first three data points downstream from the vane show only a small difference between the bold values and the $x = 3.23\,m$ values used in the previous comparison between CFD and experiment. The most significant difference is seen in the last data point, $104\,cm$ downstream from the vane. Since the vortex has almost diminished by this distance it can be argued that this difference becomes less significant. In summary, the error is small when comparing a numerical simulations of the streamwise vortex with the vane fixed at $x = 3.23\,m$, to the experimental results were the data measurement location is fixed and the vane is moved. More specifically the error for distances less than $27.9\,cm$ downstream from the vane are less than 1.5% and are shown to be as high as 6% at $53.3\,cm$ downstream. The farthest downstream data point location, $104\,cm$, does show a 22% error but at this distance the peak vorticity has decrease by 90% and the vortex has become very weak.

4.2.4. Boundary Layer Profile. One of the potential reasons for the difference between the peak vorticity between the numerical simulations and the experimental results could be the boundary layer profile. Since the vane is embedded in the boundary layer any difference in the boundary layer profile would result in more or less momentum seen by the vane which could result in a stronger or weaker vortex. A comparison between the boundary layer profile, at $x = 3.38$, of the numerical simulation to the experimental data is shown in Fig 4.13. This figure shows the boundary layer profiles for the numerical simulations using the SA and SST turbulence models. From this figure it can be seen that the SST profile matches the experimental data very well. The velocity profile generated using the SA turbulence model also matches fairly well to the experiment but not as well as the SST model. This comparison shows that the boundary layer profiles are predicted very well by the numerical simulations and are not a source for the large discrepancy between the peak vorticity observed between the experiment and numerical simulations.

4.2.5. Grid Convergence. The grid sensitivity of the embedded streamwise vortex is explored by comparing the trajectory results for coarse and fine grids. The grid resolution in the streamwise direction was evaluated first by comparing the previously computed results to those using a coarse and fine grid in the streamwise direction. The coarse grid was generated by halving the number of grid points in the streamwise, x, direction. Figure 4.14 shows the trajectory and peak vorticity from simulations where the wake grid was coarsen in the x direction and then a simulation where all of the grids were coarsen in the x direction. From this comparison it can be seen that when the wake grid
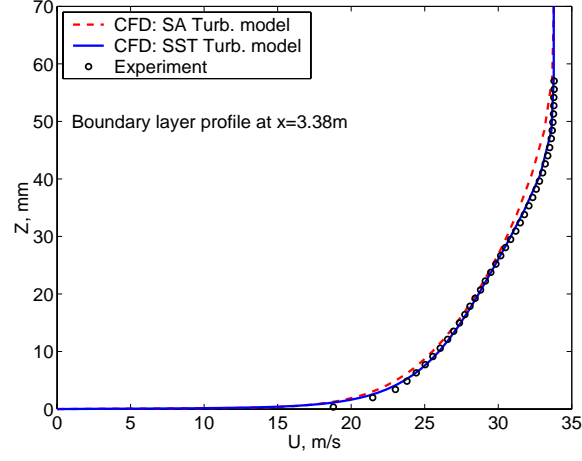
FIG. 4.13. *Boundary layer profile for the baseline flat plate flow at x = 3.38 m.*
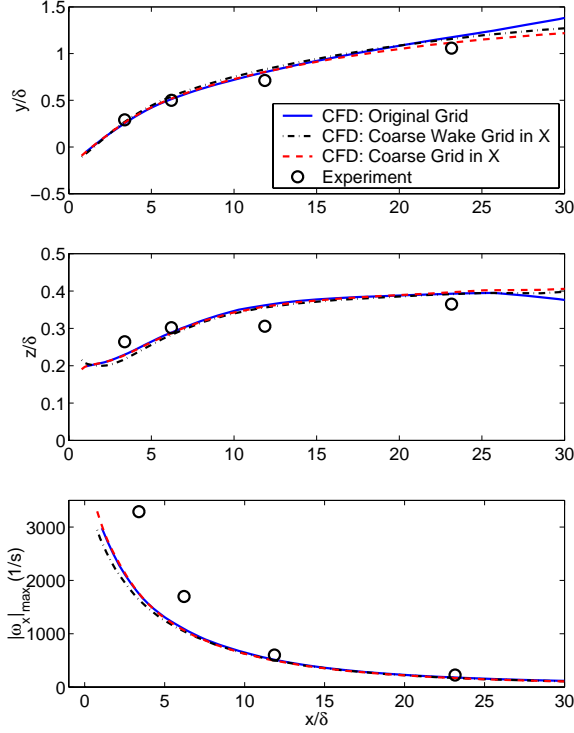

FIG. 4.14. *Grid convergence of the wake and vane grids in the streamwise direction. The wake grid which captures the vortex from the vane grids is coarsen in the streamwise directions, x, using the original vane grids. This shows that the original numerical simulation is independent of the wake grid resolution in x. The second simulation show the results from halving all of the original grids in the x direction. This simulation shows a small decreases in the peak vorticity but no significant change in the vortex trajectory. These simulations were performed using the fully modeled trapezoidal vane grids at $\alpha = 23°$.*
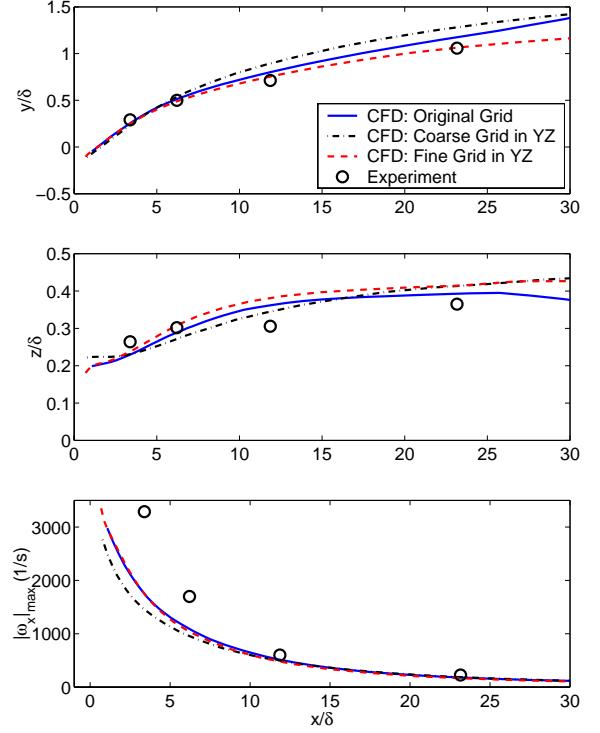
FIG. 4.15. *Grid convergence of the wake grid in the cross-stream direction This figure shows how halving the number of grid points in the cross-stream direction produces a drop in the peak vorticity. Doubling the number of grid points in the cross-stream direction results in the peak vorticity remaining the same. Both the coarse and fine grids in the cross-stream direction show a small difference in the trajectory of the streamwise vortex. In the fine grid simulation the wake grid was coarsen in the streamwise direction. These simulations were performed using the fully modeled trapezoidal vane grids at $\alpha = 23°$.*

12

is coarsen to 101 points in the streamwise direction, as compared to the original 301 points, that there is very little change in the vortex trajectory and peak vorticity. However when all of the grids are coarsen in the *x* direction there is a small drop in the peak vorticity and very little change in the path of the vortex center. This shows that the original simulation results are converge as far as the streamwise grid resolution is concerned. These results also show that the original wake grid resolution in the *x* direction can be reduced without loss of resolving the vortex peak vorticity magnitude and trajectory.

Next the grid sensitivity of the streamwise vortex in the cross-stream direction was evaluated. As in the previous case, the original numerical results were compared to the results using coarse and fine wake and vane grids. The coarse grids were generated by halving the number of grid points in the vertical, *z*, and spanwise, *y*, directions. Likewise, the fine wake grid was generated by doubling the number of grid points in the *z* and *y* directions. Due to the large number of grid points need for this simulation, the wake grid for this case had the same number of grid points in the *x* direction as was used in the previous streamwise coarse wake grid. This was done since the vortex was not effected by coarsening the wake grid in the streamwise direction. Figure 4.15 shows a comparison between the coarse and fine grids simulations in *yz* plane to the original simulation. This figure shows how the coarse grid simulation shows a small drop in the peak vorticity generated by the vane. It also shows a small difference in the trajectory of the vortex center. The simulation using the fine grids predicts the same peak vorticity with a small difference in the vortex trajectories. This result shows that the original simulation has been resolved in terms of the grid resolution in the cross-stream direction.

5. Summary. The ultimate goal of this investigation was to obtain a better understanding of the physics of a low-profile vortex generating vane and to generate numerical data of a fully modeled vane for the future development of a reduced CFD model. This was performed by simulating the vortex generating vane submerged within a turbulent boundary layer flow over a flat plate using a RANS flow solver and comparing the vane results to experimental wind tunnel PIV data. From the comparison of the vane simulations to the experimental data, it was shown that the peak vorticity of the streamwise vortex, which measures the vortex concentration, was under predicted by the RANS flow simulations. A comparison of the trajectory of the streamwise vortex in the spanwise and vertical directions showed good agreement between the numerical simulations and experiments. A comparison of the positive circulation, which measures the vortex strength, showed that the CFD and experiments agreed well except for short distances downstream of the vanes. This comparison of the circulation and peak vorticity showed that the numerical simulations were able to predict the strength of the streamwise vortex but would diffused the vortex much faster than was observed in the experiments.

It was also shown that the SST turbulence model was able to predict the vortex trajectory and peak vorticity decay much better than the SA turbulence model. The prediction of the flow for the vane at $10°$ was much better than the $23°$ case where the difference between the SA and SST models were small. From looking at the turbulent eddy viscosity, μ_t, generated by the turbulence models it was shown that the SA model had a peak μ_t at the center of the vortex where as the SST model had a minimum μ_t. This difference in the turbulent eddy viscosity would explain why simulations using the SA turbulence model displayed a more diffused vortex. The positive circulation comparisons showed that both simulations using the SA and SST turbulence models generated a streamwise vortex of equal strength. This shows that the differences in the peak vorticity are related to the diffusion of the vortex and not the vortex strength. A grid convergence study did not show any improvements in the diffusion of the streamwise vortex, showing that the diffusion of the vortex was not related to grid resolution. These results point toward the numerical scheme and the turbulence modeling as the probable source for the increased vortex diffusion seen in the numerical simulations when compared to the experiments.

The simulation of a simplified rectangular thin vane was compared to the fully modeled trapezoidal vane of finite

thickness. This comparison showed that the rectangular vane produced a streamwise vortex which was very similar to the fully grided vane. A comparison of the positive circulation also showed that they both generated streamwise vortices of equal strength. Therefore the fully grided trapezoidal vane could be replaced by a more simply grided thin vane.

REFERENCES

[1] E. E. BENDER, B. H. ANDERSON, AND P. J. YAGLE, *Vortex generator modeling for Navier-Stokes codes.* FEDSSM99-6919, 3rd Joint ASME/JSME Fluids Engineering Conference, San Francisco, CA, 1999.

[2] P. G. BUNING, D. C. JESPERSEN, T. H. PULLIAM, W. M. KLOPFER, W. M. CHAN, J. P. SLOTNICK, S. E. KRIST, AND K. J. RENZE, *OVERFLOW user's manual version 1.8m*, tech. report, NASA Langley Research Center, 1999.

[3] W. M. CHAN AND R. J. GOMEZ, *Advances in automatic overset grid generation around surface discontinuities.* AIAA 99–3303, 1999.

[4] J. W. HAMSTRA, D. N. MILLER, P. P. TRUAX, B. H. ANDERSON, AND B. J. WENDT, *Active inlet flow control technology demonstration.* ICAS-2000-6.11.2, 22nd International Congress of the Aeronautical Sciences, Harrogate, UK, 2000.

[5] D. C. JESPERSEN, *Parallelism and OVERFLOW*, Tech. Report NAS-98-013, NASA, NASA Langley Research Center, Hampton, VA 23681-2199, October 1998.

[6] D. C. JESPERSEN, T. H. PULLIAM, AND P. G. BUNING, *Vortex generator modeling for Navier-Stokes codes.* AIAA 97-0644, 1997.

[7] J. C. LIN, *Control of turbulent boundary-layer separation using micro-vortex generators.* AIAA 99–3404, 1999.

[8] F. MENTER, *Improved two-equation turbulence models for aerodynamic flows*, Tech. Report TM 103975, NASA, NASA Langley Research Center, Hampton, VA 23681-2199, 1992.

[9] T. H. PULLIAM AND D. S. CHAUSSEE, *A diagonal form of an implicit approximate-factorization algorithm*, Journal of Computational Physics, 39 (1981), pp. 347–363.

[10] P. SPALART AND S. ALLMARAS, *A one-equation turbulence model for aerodynamic flows*, La Recherche Aerospatiale, (1994), pp. 5–21.

[11] J. L. STEGER, F. C. DOUGHERTY, AND J. A. BENEK, *A chimera grid scheme*, in Advances in Grid Generation, K. N. Ghia and U. Ghia, eds., vol. 5 of FED, New York, NY, 1983, ASME.

[12] C. S. YAO, J. C. LIN, AND B. G. ALLAN, *Flowfield measurement of device-induced embedded streamwise vortex on a flat plate.* AIAA 02–3162, 2002.

REPORT DOCUMENTATION PAGE

1. AGENCY USE ONLY (Leave blank)	2. REPORT DATE May 2002	3. REPORT TYPE AND DATES COVERED Contractor Report

4. TITLE AND SUBTITLE
Simulation of embedded streamwise vortices on a flat plate

5. FUNDING NUMBERS

C NAS1-97046
WU 505-90-52-01

6. AUTHOR(S)
Brian G. Allan, Chung-Sheng Yao, and John C. Lin

7. PERFORMING ORGANIZATION NAME(S) AND ADDRESS(ES)
ICASE
Mail Stop 132C
NASA Langley Research Center
Hampton, VA 23681-2199

8. PERFORMING ORGANIZATION REPORT NUMBER

ICASE Report No. 2002-14

9. SPONSORING/MONITORING AGENCY NAME(S) AND ADDRESS(ES)
National Aeronautics and Space Administration
Langley Research Center
Hampton, VA 23681-2199

10. SPONSORING/MONITORING AGENCY REPORT NUMBER
NASA/CR-2002-211654
ICASE Report No. 2002-14

11. SUPPLEMENTARY NOTES

Langley Technical Monitor: Dennis M. Bushnell
Final Report
To appear in the Proceedings of the AIAA Flow Control Conference.

12a. DISTRIBUTION/AVAILABILITY STATEMENT

Unclassified–Unlimited
Subject Category 34, 64
Distribution: Nonstandard
Availability: NASA-CASI (301) 621-0390

12b. DISTRIBUTION CODE

13. ABSTRACT (Maximum 200 words)

Numerical simulations of a single low-profile vortex generator vane, which is only a small fraction of the boundary-layer thickness, have been performed for flows over a flat plate. The numerical simulations were computed by solving the steady-state solution to the Reynolds-averaged Navier-Stokes equations. The vortex generating vane results were evaluated by comparing the strength and trajectory of the streamwise vortex to experimental particle image velocimetry measurements. From the numerical simulations it was observed that the Shear-Stress Transport (SST) turbulence model resulted in a better prediction of the streamwise peak vorticity and trajectory when compared to the Spalart-Allmaras (SA) turbulence model. It is shown in this investigation that the estimation of the turbulent eddy viscosity near the vortex core was very high using the SA model when compared to the SST model. Even though the numerical simulations were able to predict the trajectory of the streamwise vortex, the initial magnitude and decay of the peak streamwise vorticity were significantly under predicted. A comparison of the positive circulation associated with the streamwise vortex showed that while the numerical simulations produced a more diffused vortex, that the strength of the streamwise vortex compared very well to the experimental observations. A grid resolution study was also performed showing that diffusion of the vortex was not a result of insufficient grid resolution. Comparisons were also made between a fully modeled trapezoidal vane with finite thickness to a simply modeled rectangular thin vane. These comparisons showed that the simply modeled rectangular vane produced a streamwise vortex which had a strength and trajectory very similar to the fully modeled trapezoidal vane.

14. SUBJECT TERMS
Reynolds-averaged Navier-Stokes, vortex generator

15. NUMBER OF PAGES
19

16. PRICE CODE
A03

17. SECURITY CLASSIFICATION OF REPORT Unclassified	18. SECURITY CLASSIFICATION OF THIS PAGE Unclassified	19. SECURITY CLASSIFICATION OF ABSTRACT	20. LIMITATION OF ABSTRACT